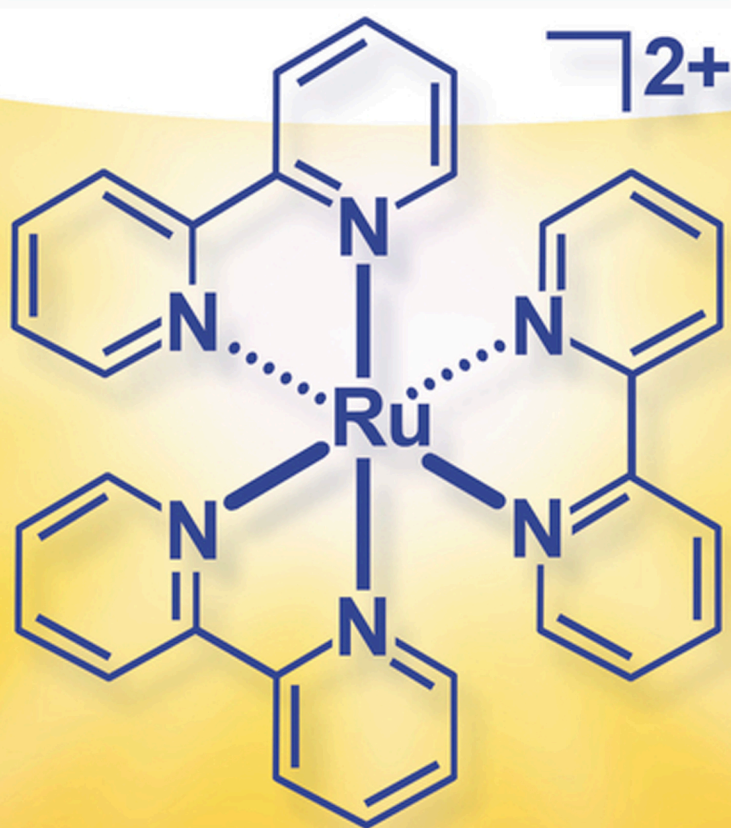


Edited by Corey R. J. Stephenson, Tehshik P. Yoon,  
and David W. C. MacMillan

# Visible Light Photocatalysis in Organic Chemistry





## **Visible Light Photocatalysis in Organic Chemistry**



# Visible Light Photocatalysis in Organic Chemistry

*Edited by Corey R. J. Stephenson, Tehshik P. Yoon,  
and David W. C. MacMillan*

WILEY-VCH

## Editors

### **Prof. Corey R. J. Stephenson**

University of Michigan  
Department of Chemistry  
930 N University Avenue  
Ann Arbor  
MI 48109  
USA

### **Prof. Tehshik P. Yoon**

University of Wisconsin-Madison  
Department of Chemistry  
1101 University Avenue  
Madison  
WI 53706  
USA

### **Prof. David W. C. MacMillan**

Princeton University  
Merck Center for Catalysis at Princeton  
NJ 08544  
USA

■ All books published by **Wiley-VCH** are carefully produced. Nevertheless, authors, editors, and publisher do not warrant the information contained in these books, including this book, to be free of errors. Readers are advised to keep in mind that statements, data, illustrations, procedural details or other items may inadvertently be inaccurate.

**Library of Congress Card No.:** applied for

### **British Library Cataloguing-in-Publication Data**

A catalogue record for this book is available from the British Library.

### **Bibliographic information published by the Deutsche Nationalbibliothek**

The Deutsche Nationalbibliothek lists this publication in the Deutsche Nationalbibliografie; detailed bibliographic data are available on the Internet at <<http://dnb.d-nb.de>>.

© 2018 Wiley-VCH Verlag GmbH & Co. KGaA, Boschstr. 12, 69469 Weinheim, Germany

All rights reserved (including those of translation into other languages). No part of this book may be reproduced in any form – by photoprinting, microfilm, or any other means – nor transmitted or translated into a machine language without written permission from the publishers. Registered names, trademarks, etc. used in this book, even when not specifically marked as such, are not to be considered unprotected by law.

**Print ISBN:** 978-3-527-33560-2

**ePDF ISBN:** 978-3-527-67417-6

**ePub ISBN:** 978-3-527-67416-9

**Mobi ISBN:** 978-3-527-67415-2

**oBook ISBN:** 978-3-527-67414-5

**Cover Design** Adam-Design, Weinheim, Germany

**Typesetting** SPi Global, Chennai, India

**Printing and Binding**

Printed on acid-free paper

## Contents

|          |   |           |
|----------|---|-----------|
| <b>1</b> | <b>An Overview of the Physical and Photophysical Properties of [Ru(bpy)<sub>3</sub>]<sup>2+</sup></b> | <b>1</b>  |
|          | <i>Daniela M. Arias-Rotondo and James K. McCusker</i>   |           |
| 1.1      | Introduction  | 1         |
| 1.2      | [Ru(bpy) <sub>3</sub> ] <sup>2+</sup> : Optical and Electrochemical Properties                        | 4         |
| 1.2.1    | Optical Properties  | 4         |
| 1.2.2    | Electrochemical Properties  | 6         |
| 1.3      | Excited State Kinetics  | 8         |
| 1.3.1    | Steady-State Emission   | 8         |
| 1.3.2    | Time-Resolved Emission  | 10        |
| 1.4      | Excited-State Reactivity of [Ru(bpy) <sub>3</sub> ] <sup>2+</sup>                                     | 11        |
| 1.5      | Energy Transfer: Förster and Dexter Mechanisms  | 12        |
| 1.6      | Electron Transfer   | 14        |
| 1.7      | Probing the Mechanism, Stage I: Stern–Volmer Quenching Studies  | 14        |
| 1.8      | Probing the Mechanism, Stage II: Electron Versus Energy Transfer                                      | 16        |
| 1.9      | Designing Photocatalysts: [Ru(bpy) <sub>3</sub> ] <sup>2+</sup> as a Starting Point                   | 20        |
| 1.10     | Conclusion  | 22        |
|          | References  | 23        |
| <b>2</b> | <b>Visible-Light-Mediated Free Radical Synthesis</b>  | <b>25</b> |
|          | <i>Louis Fensterbank, Jean-Philippe Goddard, and Cyril Ollivier</i>                                   |           |
| 2.1      | Introduction  | 25        |
| 2.2      | Basics of the Photocatalytic Cycle  | 26        |
| 2.3      | Generation of Radicals  | 27        |
| 2.3.1    | Formation of C-Centered Radicals  | 27        |
| 2.3.1.1  | Dehalogenation (I, Br, Cl)  | 27        |
| 2.3.1.2  | Other C-Heteroatom Cleavage   | 29        |
| 2.3.1.3  | C–C Bond Cleavage   | 29        |
| 2.3.2    | Formation of N-Centered Radicals  | 30        |

|          |  |           |
|----------|--|-----------|
| 2.4      | C—X Bond Formation   | 30        |
| 2.4.1    | C—O Bond   | 30        |
| 2.4.2    | C—N Bond   | 32        |
| 2.4.3    | C—S and C—Se Bonds   | 33        |
| 2.4.4    | C—Br Bond  | 34        |
| 2.4.5    | C—F Bond   | 34        |
| 2.4.6    | C—B Bond   | 35        |
| 2.5      | C—C Bond Formation   | 35        |
| 2.5.1    | Formation and Reactivity of Aryl Radicals  | 35        |
| 2.5.2    | Formation and Reactivity of Trifluoromethyl and Related Radicals                           | 40        |
| 2.5.2.1  | Photocatalyzed Reduction of Perfluorohalogen Derivatives                                   | 40        |
| 2.5.2.2  | Photocatalyzed Reduction of Perfluoroalkyl-Substituted Onium Salts                         | 42        |
| 2.5.2.3  | Photocatalyzed Formation of Perfluoroalkyl Radicals from Sulfonyl and Sulfinyl Derivatives | 43        |
| 2.5.3    | Formation and Reactivity of Alkyl and Related Radicals                                     | 45        |
| 2.5.3.1  | C—C Bond Formation Through Photocatalyzed Reduction of Halogen Derivatives and Analogs     | 45        |
| 2.5.3.2  | C—C Bond Formation Through Photocatalyzed Oxidation of Electron-Rich Functional Group      | 47        |
| 2.5.3.3  | C—C Bond Formation Through Photocatalyzed Oxidation of Amino Group                         | 48        |
| 2.6      | Radical Cascade Applications   | 49        |
| 2.6.1    | Intramolecular Polycyclization Processes   | 49        |
| 2.6.2    | Sequential Inter- and Intramolecular Processes   | 51        |
| 2.6.3    | Sequential Radical and Polar Processes   | 56        |
|          | References   | 59        |
| <b>3</b> | <b>Atom Transfer Radical Addition using Photoredox Catalysis</b>                           | <b>73</b> |
|          | <i>Theresa M. Williams and Corey R. J. Stephenson</i>                                      |           |
| 3.1      | Introduction   | 73        |
| 3.2      | Transition Metal-Catalyzed ATRA  | 77        |
| 3.2.1    | Ruthenium- and Iridium-Based ATRA  | 77        |
| 3.2.1.1  | Mechanistic Investigations   | 77        |
| 3.2.1.2  | Ruthenium- and Iridium-Based ATRA  | 80        |
| 3.2.2    | Copper-Mediated ATRA   | 81        |
| 3.2.2.1  | Trifluoromethylation   | 82        |
| 3.3      | Other Photocatalysts for ATRA Transformations  | 84        |
| 3.3.1    | <i>p</i> -Anisaldehyde   | 84        |
| 3.4      | Semiconductor  | 86        |
| 3.5      | Atom Transfer Radical Cyclization (ATRC)   | 87        |
| 3.6      | Atom Transfer Radical Polymerization (ATRP)  | 89        |
| 3.7      | Conclusion   | 90        |
|          | References   | 90        |

|          |   |            |
|----------|---|------------|
| <b>4</b> | <b>Visible Light Mediated <math>\alpha</math>-Amino C—H Functionalization Reactions</b>   | <b>93</b>  |
|          | <i>You-Quan Zou and Wen-Jing Xiao</i>   |            |
| 4.1      | Introduction  | 93         |
| 4.2      | Visible Light Mediated $\alpha$ -Amino C—H Functionalization Via Iminium Ions             | 95         |
| 4.2.1    | Aza-Henry Reaction  | 95         |
| 4.2.2    | Mannich Reaction  | 100        |
| 4.2.3    | Strecker Reaction   | 104        |
| 4.2.4    | Friedel–Crafts Reaction   | 105        |
| 4.2.5    | Alkynylation Reaction   | 108        |
| 4.2.6    | Phosphonation Reaction  | 109        |
| 4.2.7    | Addition of 1,3-Dicarbonyls   | 109        |
| 4.2.8    | Formation of C—N and C—O Bonds  | 110        |
| 4.2.9    | Miscellaneous   | 112        |
| 4.3      | Visible Light Mediated $\alpha$ -Amino C—H Functionalization Via $\alpha$ -Amino Radicals | 116        |
| 4.3.1    | Addition to Electron-Deficient Aromatics  | 116        |
| 4.3.2    | Addition to Electron-Deficient Alkenes  | 116        |
| 4.3.3    | Miscellaneous   | 120        |
| 4.4      | Conclusions and Perspectives  | 121        |
|          | References  | 122        |
| <br>     |   |            |
| <b>5</b> | <b>Visible Light Mediated Cycloaddition Reactions</b>                                     | <b>129</b> |
|          | <i>Scott Morris, Theresa Nguyen, and Nan Zheng</i>  |            |
| 5.1      | Introduction  | 129        |
| 5.2      | [2+2] Cycloadditions: Formation of Four-Membered Rings                                    | 130        |
| 5.2.1    | Introduction to [2+2] Cycloadditions  | 130        |
| 5.2.2    | Utilization of the Reductive Quenching Cycle  | 130        |
| 5.2.3    | Utilization of the Oxidative Quenching Cycle  | 135        |
| 5.2.4    | Utilization of Energy Transfer  | 139        |
| 5.2.5    | [2+2] Conclusion  | 142        |
| 5.3      | [3+2] Cycloadditions: Formation of Five-Membered Rings                                    | 143        |
| 5.3.1    | Introduction to [3+2] Cycloadditions  | 143        |
| 5.3.2    | [3+2] Cycloaddition of Cyclopropylamines  | 143        |
| 5.3.3    | 1,3-Dipolar Cycloaddition of Azomethine Ylides  | 145        |
| 5.3.4    | [3+2] Cycloaddition of Aryl Cyclopropyl Ketones   | 146        |
| 5.3.5    | [3+2] Cycloaddition via ATRA/ATRC   | 146        |
| 5.3.6    | [3+2] Conclusion  | 148        |
| 5.4      | [4+2] Cycloadditions: Formation of Six-Membered Rings                                     | 149        |
| 5.4.1    | Introduction to [4+2] Cycloadditions  | 149        |
| 5.4.2    | [4+2] Cycloadditions Using Radical Anions   | 149        |
| 5.4.3    | [4+2] Cycloadditions Using Radical Cations  | 151        |
| 5.4.4    | [4+2] Conclusion  | 154        |
| 5.5      | Conclusion  | 155        |
|          | References  | 156        |

|          |  |            |
|----------|--|------------|
| <b>6</b> | <b>Metal-Free Photo(redox) Catalysis</b>   | <b>159</b> |
|          | <i>Kirsten Zeitler</i>   |            |
| 6.1      | Introduction   | 159        |
| 6.1.1    | Background   | 162        |
| 6.1.2    | Classes of Organic Photocatalysts  | 162        |
| 6.2      | Applications of Organic Photocatalysts   | 166        |
| 6.2.1    | Energy Transfer Reactions  | 166        |
| 6.2.2    | Reductive Quenching of the Catalyst  | 171        |
| 6.2.2.1  | Cyanoarenes  | 171        |
| 6.2.2.2  | Quinones   | 172        |
| 6.2.2.3  | Cationic Dyes: Pyrylium, Quinolinium, and Acridinium Scaffolds                       | 173        |
| 6.2.2.4  | Xanthene Dyes and Further Aromatic Scaffolds   | 188        |
| 6.2.3    | Oxidative Quenching of the Catalyst  | 203        |
| 6.2.4    | New Developments   | 214        |
| 6.2.4.1  | Upconversion   | 215        |
| 6.2.4.2  | Consecutive Photoelectron Transfer   | 215        |
| 6.2.4.3  | Multicatalysis   | 216        |
| 6.3      | Conclusion and Outlook   | 224        |
|          | References   | 224        |
| <br>     |  |            |
| <b>7</b> | <b>Visible Light and Copper Complexes: A Promising Match in Photoredox Catalysis</b> | <b>233</b> |
|          | <i>Suva Paria and Oliver Reiser</i>  |            |
| 7.1      | Introduction   | 233        |
| 7.2      | Photophysical Properties of Copper Catalysts   | 234        |
| 7.3      | Application of Copper Based Photocatalysts in Organic Synthesis                      | 237        |
| 7.4      | Outlook  | 247        |
|          | Acknowledgment   | 248        |
|          | References   | 248        |
| <br>     |  |            |
| <b>8</b> | <b>Arene Functionalization by Visible Light Photoredox Catalysis</b>                 | <b>253</b> |
|          | <i>Durga Hari Prasad, Thea Hering, and Burkhard König</i>                            |            |
| 8.1      | Introduction   | 253        |
| 8.1.1    | Aryl Diazonium Salts   | 253        |
| 8.1.2    | Diaryl Iodonium Salts  | 268        |
| 8.1.3    | Triaryl Sulfonium Salts  | 272        |
| 8.1.4    | Aryl Sulfonyl Chlorides  | 273        |
| 8.2      | Applications of Aryl Diazonium Salts   | 274        |
| 8.3      | Photoinduced Ullmann C—N Coupling  | 276        |
| 8.4      | Conclusion   | 278        |
|          | References   | 278        |

- 9 Visible-Light Photocatalysis in the Synthesis of Natural Products** 283  
*Gregory L. Lackner, Kyle W. Quasdorf, and Larry E. Overman*  
References 295
- 10 Dual Photoredox Catalysis: The Merger of Photoredox Catalysis with Other Catalytic Activation Modes** 299  
*Christopher K. Prier and David W. C. MacMillan*
- 10.1 Introduction 299
- 10.2 Merger of Photoredox Catalysis with Organocatalysis 300
- 10.3 Merger of Photoredox Catalysis with Acid Catalysis 314
- 10.3.1 Photoredox Catalysis and Brønsted Acid Catalysis 314
- 10.3.2 Photoredox Catalysis and Lewis Acid Catalysis 318
- 10.4 Merger of Photoredox Catalysis with Transition Metal Catalysis 320
- 10.5 Conclusions 328  
References 328
- 11 Enantioselective Photocatalysis** 335  
*Susannah C. Coote and Thorsten Bach*
- 11.1 Introduction 335
- 11.2 The Twentieth Century: Pioneering Work 336
- 11.3 The Twenty-First Century: Contemporary Developments 341
- 11.3.1 Large-Molecule Chiral Hosts 341
- 11.3.2 Small-Molecule Chiral Photosensitizers 343
- 11.3.3 Lewis Acid-Mediated Photoreactions 353
- 11.4 Conclusions and Outlook 357  
References 358
- 12 Photomediated Controlled Polymerizations** 363  
*Nicolas J. Treat, Brett P. Fors, and Craig J. Hawker*
- 12.1 Catalyst Activation by Light 365
- 12.1.1 Cu-Catalyzed Photoregulated Atom Transfer Radical Polymerizations (photoATRP) 365
- 12.1.2 Photomediated ATRP with Non-Copper-Based Catalyst Systems 368
- 12.1.3 Iodine-Mediated Photopolymerizations 371
- 12.1.4 Metal-Free Photomediated Ring-Opening Metathesis Polymerization 375
- 12.1.5 Photoregulated Reversible-Addition Fragmentation Chain Transfer Polymerizations (photoRAFT) 376
- 12.2 Chain-End Activation by Light 383
- 12.3 Conclusions 384  
References 385

|           |   |            |
|-----------|---|------------|
| <b>13</b> | <b>Accelerating Visible-Light Photoredox Catalysis in Continuous-Flow Reactors</b>                      | <b>389</b> |
|           | <i>Natan J. W. Straathof and Timothy Noël</i>   |            |
| 13.1      | Introduction  | 389        |
| 13.2      | Homogeneous Photocatalysis in Single-Phase Flow   | 392        |
| 13.3      | Gas–liquid Photocatalysis in Flow   | 401        |
| 13.4      | Heterogeneous Photocatalysis in Flow  | 408        |
| 13.5      | Conclusions   | 410        |
|           | Conflict of Interest  | 410        |
|           | References  | 410        |
| <br>      |   |            |
| <b>14</b> | <b>The Application of Visible-Light-Mediated Reactions to the Synthesis of Pharmaceutical Compounds</b> | <b>415</b> |
|           | <i>James. J. Douglas</i>  |            |
| 14.1      | Introduction  | 415        |
| 14.2      | Asymmetric Benzylation  | 415        |
| 14.3      | Amide Bond Formation  | 416        |
| 14.4      | C–H Azidation   | 417        |
| 14.5      | Visible-Light-Mediated Benzothiophene Synthesis   | 418        |
| 14.6      | $\alpha$ -Amino Radical Functionalization   | 419        |
| 14.7      | Visible-Light-Mediated Radical Smiles Rearrangement   | 422        |
| 14.8      | Photoredox and Nickel Dual Catalysis  | 423        |
| 14.9      | The Scale-Up of Visible-Light-Mediated Reactions Via Continuous Processing                              | 426        |
|           | References  | 428        |
| <br>      |   |            |
|           | <b>Index</b>  | <b>431</b> |

# An Overview of the Physical and Photophysical Properties of $[\text{Ru}(\text{bpy})_3]^{2+}$

Daniela M. Arias-Rotondo and James K. McCusker

Michigan State University, Department of Chemistry, 578 S Shaw Lane, East Lansing, MI 48824, United States

## 1.1 Introduction

The photophysics and photochemistry of transition-metal coordination compounds have been studied for over half a century [1, 2]. In particular, metal polypyridyl complexes – especially those that possess visible charge transfer absorptions – have played a central role in efforts to understand fundamental aspects of excited-state electronic structure and dynamics, as well as efforts to develop a wide range of solar energy conversion strategies [3, 4]. Their footprint in the area of synthetic organic chemistry was largely nonexistent until 2008 [5], when MacMillan and coworkers [6] reported the first example of a transition-metal-based charge transfer compound,  $[\text{Ru}(\text{bpy})_3]^{2+}$  (where bpy is 2,2'-bipyridine), acting as a photocatalyst (PC) in an asymmetric alkylation of aldehydes; simultaneously, Yoon and coworkers [7] reported [2+2] enone cycloadditions photocatalyzed by  $[\text{Ru}(\text{bpy})_3]^{2+}$ . Following those initial reports, several groups have explored the use of coordination compounds as photocatalysts for a variety of organic transformations [8]. These compounds engage in single-electron transfer (SET) processes with organic substrates, generating organic radicals, which play a major role in organic synthesis. This new kind of catalysis has opened the door to synthetically useful reactions that could not be performed otherwise.

The majority of the photocatalysts used nowadays are polypyridyl complexes of either Ru(II) or Ir(III) [8]. The large number of examples using  $[\text{Ru}(\text{bpy})_3]^{2+}$  might make this compound look like a “one size fits all” photocatalyst, when in reality, the best photocatalyst for a reaction is determined by the kinetics and thermodynamics of the system of interest. The purpose of this chapter is to provide the necessary tools to understand the different factors that come into play when choosing a photocatalyst. To this end, we will use  $[\text{Ru}(\text{bpy})_3]^{2+}$  as an example; it is important to note that the concepts we will discuss apply to most transition-metal polypyridyl compounds.

\* An expanded discussion of these topics can be found in Chem. Soc. Rev. 2016, 45, 5803–5820.

Scheme 1.1 shows two examples of catalytic cycles using Ru(II)-based photoredox catalysts: in both cases, the first step is the absorption of a photon by the photocatalyst to generate an excited state that then engages in redox reactions. The first cycle in Scheme 1.1, reported by Zheng and coworkers [9], is called reductive, because the excited photocatalyst is reduced. The second one, reported by Cano-Yelo and Deronzier [10], is an oxidative cycle; the photocatalyst is first oxidized and then reduced to reform its resting state.

As shown in Scheme 1.1, most steps in a catalytic cycle are bimolecular reactions. In a very general way, for any catalytic cycle involving  $[\text{Ru}(\text{bpy})_3]^{2+}$ , we can write the series of reactions in Scheme 1.2 [11, 12]. The first step is the absorption of a visible light photon by the photocatalyst in its ground state and its consequent promotion to an electronic excited state ( $\text{PC}^*$ ); the backward reaction is the ground-state recovery (this process can be radiative (i.e., emission) and/or nonradiative, as will be discussed in Section 1.3). For the excited photocatalyst to react with a molecule (R), both species must diffuse toward each other, forming a “precursor complex.” Then, the reaction takes place; of the many kinds of reactions that could happen, only electron and energy transfer are relevant for our discussion. After the reaction, the products must diffuse away from each other; if they cannot escape the solvent cage fast enough, a back reaction may take place.

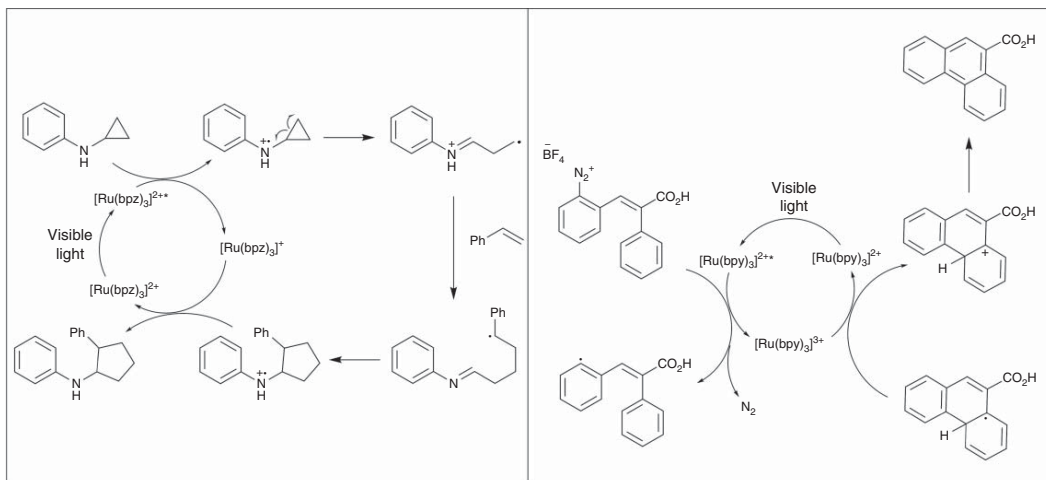
This relatively simple scheme allows us to outline the main points that need to be considered when choosing a photocatalyst:

- 1) Photocatalytic reactions make use of the enhanced reactivity of the photocatalyst in its excited state; for this reason, a photocatalyst must possess a good absorption cross section, preferably over a broad range of wavelengths that the other species in the reaction mixture do not absorb.<sup>1</sup>
- 2) The quantum yield of formation of the reactive excited state should be as high as possible (preferably, near unity); that state must persist long enough to undergo the desired reaction with the substrate, and then cleanly regenerate in order to maintain its viability as part of a catalytic cycle. In the context of Scheme 1.2, these latter criteria mean that  $k_d$  and  $k_q$  must be larger than  $k_0$ , so that the  $\text{PC}^*$  can diffuse toward the appropriate molecule and react with it before going back to the ground state [13].
- 3) If the catalytic cycle involves electron transfer, the excited- and ground-state redox potentials of the photocatalyst must provide for an exothermic (or at worst weakly endothermic) reaction; reversible electrochemistry is also desirable as an indicator of the stability of the photocatalyst over multiple turnovers.<sup>2</sup>
- 4) Synthetic accessibility and, more importantly, tunability are critical in order to tailor the excited-state reactivity of the photocatalyst to the reaction of interest.

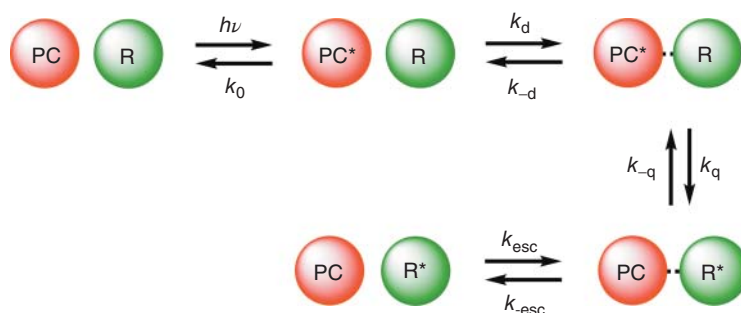
---

1 Strictly speaking, it is only necessary for the photocatalyst to absorb light of one wavelength that the other species present in the reaction mixture do not absorb; having the photocatalyst absorb over a wider range of wavelengths makes it more versatile.

2 This is not necessary in the case of an energy-transfer photocatalyst, but those are far less common (see Prier, C. K.; Rankic, D. A.; MacMillan, D. W. *op. cit.* and references therein).



**Scheme 1.1** Examples of reductive catalytic cycle (left; see also [9]) and oxidative catalytic cycle (right; see also [10]) involving Ru(II)-based photocatalysts; bpz is 2,2'-bipyrazine.



**Scheme 1.2** Simplified kinetic scheme for a general quenching process (see also [11, 12]).

Given the various criteria just enumerated, it is no surprise that polypyridyl complexes of Ru(II) and Ir(III) have proved useful as photoredox catalysts. These compounds strongly absorb visible light, which makes it easy to selectively excite them relative to the organic substrates for typical reactions of interest. Their excited states are formed with  $\sim 100\%$  efficiency [14] and their lifetimes range from 300 ns to 6  $\mu\text{s}$ , which is long enough for them to engage in bimolecular reactions [3, 15]. As a class, these compounds are generally stable with respect to decomposition (both photochemical and thermal) and typically exhibit reversible redox behavior. They are also emissive, which facilitates mechanistic studies (as discussed in Sections 1.7 and 1.8); however, it is not a requirement. The synthesis of transition-metal polypyridyl complexes has been studied in great detail [4, 16], as well as the effect that different ligands have on the properties of the ground and excited states [17]. All these properties make these compounds the preferred choice for photocatalysts.

As mentioned above, we will discuss the properties of the ground and excited states of  $[\text{Ru}(\text{bpy})_3]^{2+}$ , as a prototype for photoredox catalysis, describing the necessary experiments to fully understand their properties. Using this as a foundation, we will then focus on the processes that take place during a photocatalytic cycle and the experiments that allow for discriminating between various mechanistic possibilities (the main question being energy transfer versus reductive/oxidative electron transfer). In so doing, our goal is to provide a basic blueprint for how to identify, characterize, and ultimately design photocatalysts for use in a wide variety of chemical transformations.

## 1.2 $[\text{Ru}(\text{bpy})_3]^{2+}$ : Optical and Electrochemical Properties

### 1.2.1 Optical Properties

The electronic absorption spectrum of  $[\text{Ru}(\text{bpy})_3](\text{PF}_6)_2$  in acetonitrile is shown in Figure 1.1. The intense absorption at 285 nm corresponds to a ligand-centered transition ( $\pi_{\text{L}} \rightarrow \pi_{\text{L}}^*$ ), which has been assigned by comparison with the absorption spectrum of the protonated ligand [18]. The band in the visible region

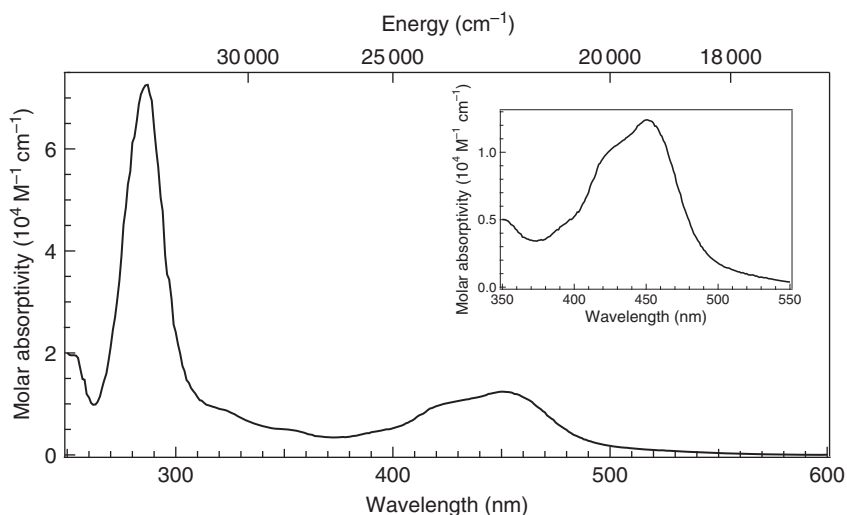
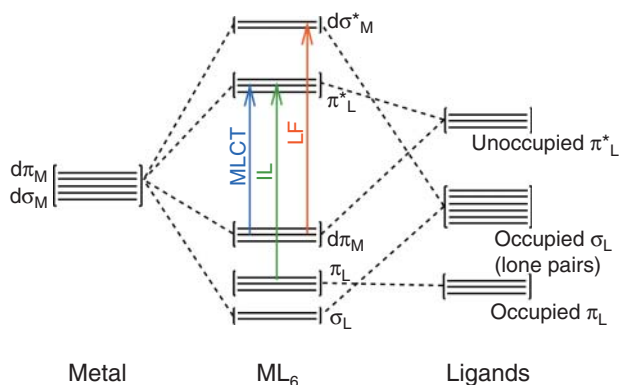


**Figure 1.1** Electronic absorption spectrum of [Ru(bpy)<sub>3</sub>](PF<sub>6</sub>)<sub>2</sub> in acetonitrile at room temperature. The inset shows the metal-to-ligand charge transfer (MLCT) band.

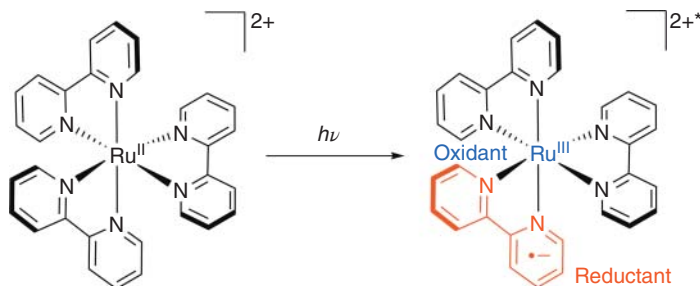
( $\lambda_{\text{max}} = 452 \text{ nm}$ ) corresponds to a metal-to-ligand charge transfer (MLCT) transition. As the name implies, this type of excited state can be viewed as the promotion of an electron from a metal-based orbital to a ligand-based one. Because of this spatial redistribution of electron density, this transition is responsible for the enhanced redox activity of the excited state relative to what is observed in the ground state, and makes the compound an efficient photocatalyst. Charge transfer transitions are typically very intense, with extinction coefficients in the range of  $10^3$  to  $10^4 \text{ M}^{-1} \text{ cm}^{-1}$  [19] (in acetonitrile at room temperature,  $\epsilon \sim 15\,000 \text{ M}^{-1} \text{ cm}^{-1}$  for [Ru(bpy)<sub>3</sub>]<sup>2+</sup>).

Two additional features can be seen in the absorption spectrum of [Ru(bpy)<sub>3</sub>]<sup>2+</sup>. The origin(s) of the weaker features at 330 and 350 nm are less clear-cut and have been the subject of considerable debate over the years. They are most likely due to ligand–field (so-called “d–d”) transitions within the d-orbital manifold of the metal. The inferred intensity belies this assignment to a certain extent (the symmetry-forbidden nature of d–d bands typically limits their absorptivities to the range of  $10$ – $100 \text{ M}^{-1} \text{ cm}^{-1}$ ) [19] but the proximity of both the ligand-centered and MLCT features influences these values in the present case. These metal-centered transitions put electronic density in orbitals that are antibonding with respect to the metal–ligand bonds and are therefore responsible for ligand loss reactions [3]. These three types of transitions are schematized in the simplified molecular orbital diagram in Scheme 1.3.

It is worth noting that most organic substrates, with the exception of highly conjugated systems, do not absorb visible light (cf. ligand-based transition in Figure 1.1). Thus, the use of visible light allows the selective excitation of the photocatalyst and not the organic reactants, which prevents the uncontrolled formation of organic radicals that could lead to unwanted side reactions.



**Scheme 1.3** Simplified molecular orbital diagram for an octahedral compound with  $\pi$ -acceptor ligands. The three types of electronic transitions discussed in the text are indicated by the arrows.



**Scheme 1.4** A qualitative representation of a metal-to-ligand charge transfer state in  $[\text{Ru}(\text{bpy})_3]^{2+}$ . The spatial separation of charge within the molecule following light absorption is critical for the redox activity of the excited state.

A metal-to-ligand charge transfer transition can be thought of as the simultaneous oxidation of the metal center and reduction of the ligand [20] that yields  $[\text{Ru}^{\text{III}}(\text{bpy}^{\bullet-})(\text{bpy})_2]^{2+*}$  (see Scheme 1.4). Unlike ligand- or metal-based electronic transitions (where the electron stays in the same spatial region before and after excitation), the MLCT results in the separation of charges within the compound, which confers a special reactivity to the resulting state: the oxidized metal ( $\text{Ru}^{\text{III}}$ ) can act as an oxidant, gaining an electron to form  $\text{Ru}^{\text{II}}$ ; likewise, the reduced ligand ( $\text{bpy}^{\bullet-}$ ) can donate its extra electron, acting as a reductant. In its excited state,  $[\text{Ru}(\text{bpy})_3]^{2+*}$  is both a stronger oxidant and reductant than in its ground state. Moreover, both the reductant and oxidant are simultaneously present in the same molecule, making this class of compounds very versatile for applications in photocatalysis.

## 1.2.2 Electrochemical Properties

Most of the examples using transition-metal photocatalysts take advantage of their ground- and excited-state redox properties. It is thus important to

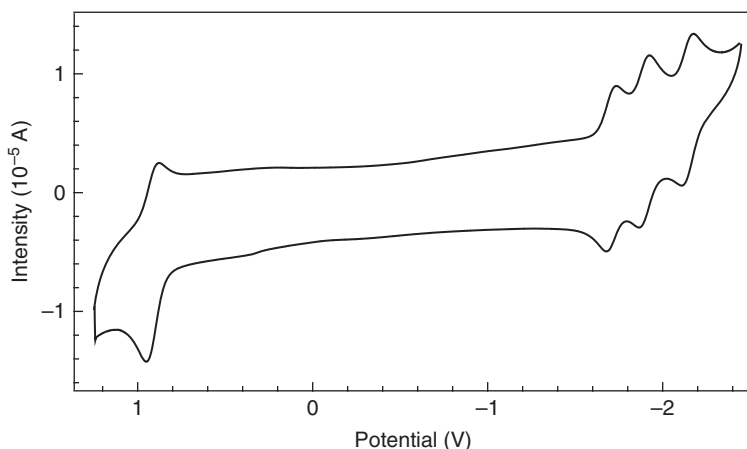
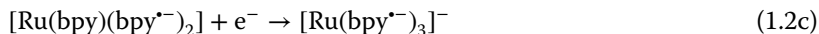
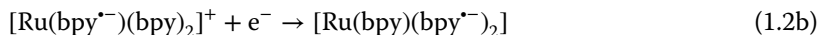
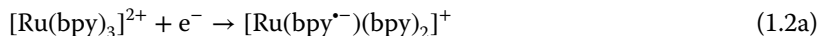


**Figure 1.2** Cyclic voltammogram of  $[\text{Ru}(\text{bpy})_3](\text{PF}_6)_2$  in  $\text{CH}_3\text{CN}$  solution, using 0.1 M tetrabutylammonium hexafluorophosphate ( $\text{TBAPF}_6$ ) as supporting electrolyte. Potentials are referenced to the ferrocene/ferrocenium couple, added as an internal standard.

understand those properties and how they affect the behavior of  $[\text{Ru}(\text{bpy})_3]^{2+}$  as a photocatalyst. The redox potentials for a coordination compound such as  $[\text{Ru}(\text{bpy})_3]^{2+}$  can be measured using cyclic voltammetry. The cyclic voltammogram for  $[\text{Ru}(\text{bpy})_3](\text{PF}_6)_2$  is shown in Figure 1.2. The oxidation of the metal center (Eq. (1.1)) is reversible and takes place around 1.00 V (vs. ferrocene/ferrocenium).



Three reductions are also observed in the  $-1.50$  to  $-2.30$  V range, all of which correspond to one-electron reductions of each of the three ligands in succession (Eqs. (1.2a–1.2c)).



The first two reductions are reversible, whereas the last one (Eq. (1.2c)) is quasi-reversible at best. In terms of photoredox reactions, only the first reduction (i.e., Eq. (1.2a)) will be relevant for one-electron processes, but the reversibility of these redox processes is an important consideration when these compounds are used as photocatalysts, since the compound must be stable enough in its oxidized or reduced form in order to be viable over the course of multiple turnovers of a given reaction.

Using the description above, the energy of the MLCT band can be thought of as the amount of energy necessary to reduce the ligand and oxidize the metal, as shown in Eq. (1.3).

$$E(\text{MLCT}) \approx |E(\text{Ru}^{\text{III}}/\text{Ru}^{\text{II}})| + |E(\text{bpy}/\text{bpy}^{\bullet-})| \quad (1.3)$$

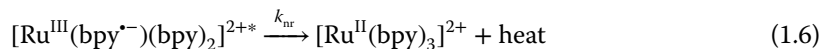
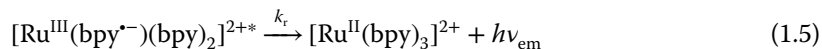
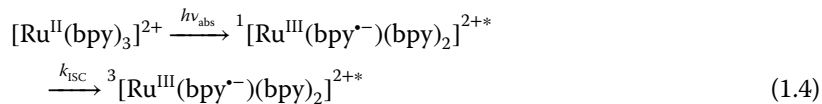
Several aspects of Eq. (1.3) are worth noting: (i) this is an approximation: energetics associated with solvation as well as electron correlation effects are not accounted for in this simplified expression [21]; (ii) the fact that there are two contributions to the MLCT energy – the oxidation potential of the metal and the reduction potential of the ligand – implies that the value of  $E(\text{MLCT})$  alone is not sufficient to determine whether a chromophore's energetics are suitable for a given reaction. One can observe MLCT bands at roughly the same energy where one is a very strong reductant but a very weak oxidant (i.e., very negative ligand reduction potential), or vice-versa. The electrochemical data on the compound (in addition to other details to be discussed later) is the means by which these specifics can be deconvolved.

### 1.3 Excited State Kinetics

We are ultimately interested in bimolecular reactions between an excited photocatalyst and an organic molecule. Before we can discuss these bimolecular reactions, however, it is necessary to understand the properties of the excited state in the absence of a substrate, since the presence (or absence) of a reaction will ultimately be determined by referring back to the photocatalysts' intrinsic excited-state behavior.

#### 1.3.1 Steady-State Emission

Visible light excites  $[\text{Ru}(\text{bpy})_3]^{2+}$  into an  $^1\text{MLCT}$  state; this short-lived state relaxes to an  $^3\text{MLCT}$  state within  $\sim 100$  fs via intersystem crossing (ISC, with rate constant  $k_{\text{isc}}$ ) [22]. The  $^3\text{MLCT}$  state can relax back to the ground state either nonradiatively (with rate constant  $k_{\text{nr}}$ ) or via phosphorescence (a radiative pathway; its rate constant is  $k_{\text{r}}$ ). Equations (1.4)–(1.6) illustrate these processes. Photoinduced reactions, such as the coordination of a solvent molecule or ligand loss, can also take place. However, these are not usually observed for  $[\text{Ru}(\text{bpy})_3]^{2+}$  and related compounds [14], so they will not be discussed here.



The solution-phase steady-state emission spectrum of  $[\text{Ru}(\text{bpy})_3]^{2+}$  at room temperature is shown in Figure 1.3: the emission maximum is at 620 nm. The same spectrum is obtained regardless of the excitation wavelength, consistent with the near-unit quantum yield of formation of the emissive  $^3\text{MLCT}$  state. The emission maximum can be used as a first-order approximation of the energy difference between the triplet excited state ( $^3\text{MLCT}$ ) and the ground state (the zero point energy,  $E_0$ ).

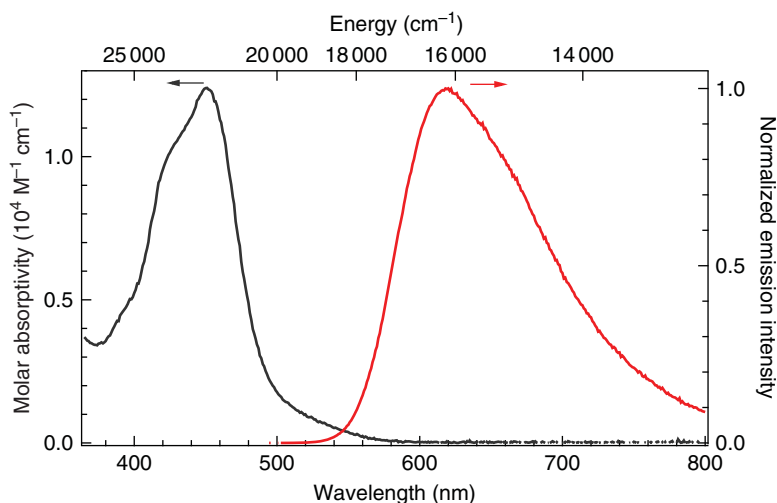


**Figure 1.3** Electronic absorption spectrum (black) and steady-state emission spectrum (red) of  $[\text{Ru}(\text{bpy})_3](\text{PF}_6)_2$  in acetonitrile at room temperature.

For an emissive substance, the simplest definition of the quantum yield ( $\Phi$ ) of emission (also called the radiative quantum yield) is the ratio between the number of photons emitted by a sample and the number of photons absorbed, as shown in Eq. (1.7).

$$\Phi = \frac{\# \text{ photons emitted}}{\# \text{ photons absorbed}} = \frac{I_{\text{em}}}{I_{\text{abs}}} \quad (1.7)$$

For every photon absorbed, one molecule is promoted to the excited state. The radiative quantum yield can also be described in terms of a kinetic competition, specifically the relative rate(s) of processes giving rise to emission versus the rates of all processes that serve to deplete the population of that emissive state. Referring to Eqs. (1.5) and (1.6), for  $[\text{Ru}(\text{bpy})_3]^{2+}$  in the absence of any other species,  $\Phi$  can be expressed as

$$\Phi_0 = \frac{k_r}{k_r + k_{\text{nr}}} = \frac{k_r}{k_0} \quad (1.8)$$

Radiative quantum yields can be measured as absolute values (i.e., Eq. (1.7)) or relative to some standard. To measure an absolute quantum yield it is necessary to detect every photon that is emitted by the sample, which tends to be quite labor intensive. Although instrumentation has recently become commercially available to allow for (relatively) facile measurement of absolute radiative quantum yields,<sup>3</sup> most of the quantum yields in literature are determined and reported relative to a standard with a known absolute quantum yield [23]. The choice of the standard depends on the characteristics of the molecule of interest; it is best if the standard and the molecule are dissolved in the same solvent and have similar absorption and emission spectra.  $[\text{Ru}(\text{bpy})_3]^{2+}$  is commonly used as a standard for relative

<sup>3</sup> <http://www.hamamatsu.com>.

quantum yields of transition-metal complexes. In deoxygenated<sup>4</sup> acetonitrile at room temperature its quantum yield is 0.095 [24]. The relative quantum yield of a sample can be calculated using Eq. (1.9),

$$\Phi_x = \Phi_{\text{std}} \left( \frac{I_x/A_x}{I_{\text{std}}/A_{\text{std}}} \right) \left( \frac{\eta_x}{\eta_{\text{std}}} \right)^2 \quad (1.9)$$

where  $x$  refers to the molecule of interest and  $\text{std}$  to the standard;  $I_x$  and  $I_{\text{std}}$  are the integrated areas of the corrected emission spectra,<sup>5</sup>  $A_x$  and  $A_{\text{std}}$  are the absorbances at the excitation wavelength, and  $\eta_x$  and  $\eta_{\text{std}}$  are the indexes of refraction of the solutions, taken to be equal to those of the neat solvents. For relative quantum yield determinations, it is crucial for the experimental conditions for both the sample and the standard to be exactly the same. A more detailed discussion of methodology for measuring and quantifying emission data is beyond the scope of this chapter, but a number of excellent resources are readily available [25, 26].

As will be discussed later, observing a change (specifically, an attenuation) in the quantum yield of emission of a photocatalyst in the presence of a quencher is an important initial indicator that a reaction is occurring between the excited state of the photocatalyst and one or more substrate(s).

### 1.3.2 Time-Resolved Emission

Both the radiative and nonradiative decay processes (Eqs. (1.5) and (1.6)) are of first order with respect to the excited state (ES) and give rise to the following rate expression for the loss of the excited state:

$$-\frac{d[\text{ES}]}{dt} = k_r [\text{ES}] + k_{\text{nr}} [\text{ES}] = (k_r + k_{\text{nr}})[\text{ES}] = k_0 [\text{ES}] \quad (1.10)$$

where  $k_0 = k_{\text{nr}} + k_r$ . Equation (1.10) can be integrated to yield the known rate law for a first-order reaction, shown in Eq. (1.11).

$$[\text{ES}] = [\text{ES}]_0 e^{-k_0 t} \quad (1.11)$$

The inverse of the observed rate constant,  $k_0^{-1}$ , is the lifetime ( $\tau_0$ ) of the excited state; experimentally, this can be measured with time-resolved emission or absorption spectroscopy.

In a time-resolved emission experiment, the (emissive) sample is excited at a wavelength close to its absorption maximum, with the emission collected at  $90^\circ$  with respect to the excitation beam in order to minimize scatter. A typical time-resolved emission trace for  $[\text{Ru}(\text{bpy})_3]^{2+}$  in acetonitrile is shown in Figure 1.4. By fitting the trace to an exponential decay,  $\tau_0$  can be found. For  $[\text{Ru}(\text{bpy})_3]^{2+}$ , the lifetime ranges from 500 to 1000 ns, depending on a number of variables including solvent, oxygen concentration in the sample, temperature, and so on [3].

<sup>4</sup> This is necessary because  $\text{O}_2$  can quench the <sup>3</sup>MLCT excited state of  $[\text{Ru}(\text{bpy})_3]^{2+}$ .

<sup>5</sup> Spectra refer to emission spectra that have been properly corrected for the fluorimeter's instrument response characteristics. References on emission spectroscopy can be consulted for further information on this point.

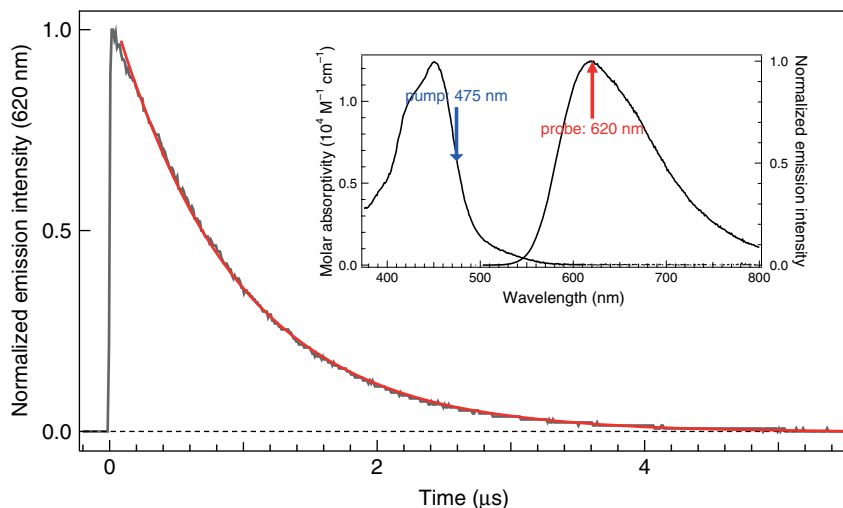


**Figure 1.4** Time-resolved emission data (grey line) for  $[\text{Ru}(\text{bpy})_3]^{2+}$  in acetonitrile at room temperature. The sample was excited at 475 nm and emission was detected at 620 nm (as shown in the inset). The red trace shows the fit to a single exponential decay with  $\tau = 930$  ns.

Combining the excited-state lifetime and the quantum yield, it is possible to calculate  $k_r$  and  $k_{nr}$ . Rearranging Eq. (1.8), we obtain Eqs. (1.12) and (1.13).

$$k_r = \Phi_0 \times k_0 \quad (1.12)$$

$$k_{nr} = k_0 - (\Phi_0 \times k_0) \quad (1.13)$$

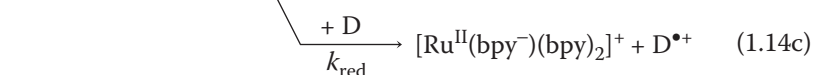
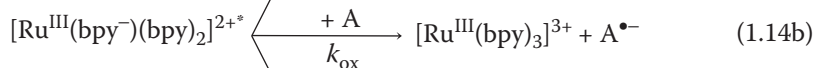
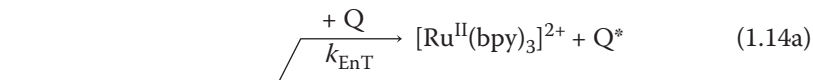
It is important to remark that  $k_r$  is an intrinsic property of the molecule, and as such, it remains constant no matter what reactions the excited state engages in. On the other hand,  $k_{nr}$  varies when quenching processes (such as energy or electron transfer) take place. All the information that we will be interested in for a photocatalytic cycle (in other words, the information about any processes competing with the emission) is contained in  $k_{nr}$ ; in this regard,  $k_r$  can be viewed as a probe, providing insight into the dynamics of the system manifesting in  $k_{nr}$ . This concept is discussed in greater detail in Section 1.7.

## 1.4 Excited-State Reactivity of $[\text{Ru}(\text{bpy})_3]^{2+}$

In its excited state,  $[\text{Ru}(\text{bpy})_3]^{2+}$  can act as an energy donor, an electron acceptor, or an electron donor; which of these processes dominates is determined by thermodynamic and kinetic factors associated with a given reaction [27].

The inherent competition that exists among these various reaction pathways is depicted in Eqs. (1.14a–1.14c); the energy transfer route can furthermore be subdivided according to the specific mechanism of that process. As a result, although determining whether the excited state of the chromophore is reacting can be as straightforward as observing emission quenching, mechanistic discrimination as to the nature of that reaction generally requires considerably more work. The next

sections will discuss these different processes and describe experiments that are typically employed in order to distinguish among them.



## 1.5 Energy Transfer: Förster and Dexter Mechanisms

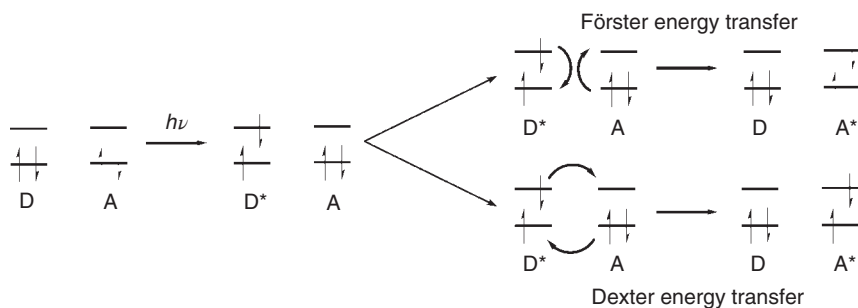
Energy transfer is a process by which excess energy contained in one molecule (the donor) is transferred to another molecule (the acceptor). In the context of the chemical systems being discussed herein, that excess energy comes from the absorption of a photon by the donor to create an electronic excited state. The product of the reaction is an electronically excited acceptor molecule concomitant with reformation of the electronic ground state of the donor, as shown in Eq. (1.15).



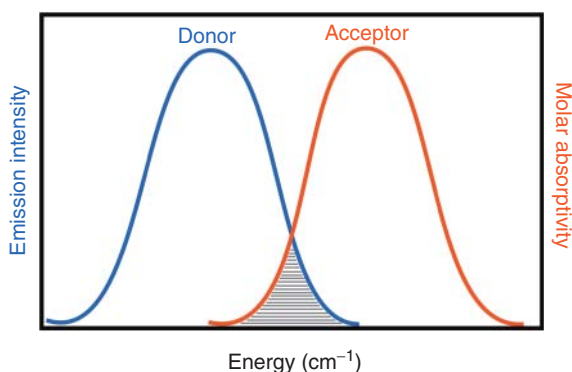
Although energy transfer can occur as the result of emission from the donor and subsequent absorption of that emitted light by the acceptor (the so-called “trivial” mechanism), energy transfer more typically occurs via nonradiative processes (i.e., the emission and reabsorption of light do not occur). The two most common mechanisms of nonradiative energy transfer are known as Förster (through-space) and Dexter (through-bond or “exchange”) energy transfer. These mechanisms are depicted in Scheme 1.5. It should be noted that both Förster and Dexter transfers yield the same products (i.e., ground-state donor and excited-state acceptor), although the physical origins of the reaction are fundamentally different [28].

Förster energy transfer [29] is a dipolar mechanism that takes place through space: the transition moment dipole of the donor couples nonradiatively with the transition moment dipole of the acceptor. Because of the dipolar nature of this mechanism, no orbital overlap is necessary between the donor and the acceptor. This makes Förster energy transfer operational at long distances that can range from 1 to 10 nm [30]. In the photosynthetic apparatus, the energy absorbed by the antenna complex is shuttled to the reaction center via Förster energy transfer [31].

An overlap between the emission spectrum of the donor and the electronic absorption spectrum of the acceptor is necessary for the energy transfer to occur: for this reason, Förster transfer is often referred to as fluorescence resonance energy transfer, or FRET. A schematic representation of this resonance condition (which in reality is simply a reflection of energy conservation for the energy transfer process) is shown in Scheme 1.6. The organic reactants usually involved



**Scheme 1.5** Förster and Dexter energy transfer mechanisms.



**Scheme 1.6** Schematic emission spectrum of the donor and absorption spectrum of the acceptor. The shaded region is the spectral overlap.

in photocatalyzed reactions do not readily absorb light in the visible region of the spectrum, so the spectral overlap between their absorption spectrum and the emission spectrum of  $[\text{Ru}(\text{bpy})_3]^{2+}$  is usually negligible. As a consequence, Förster energy transfer is not a common reaction pathway for the systems that are discussed in this chapter.

The Dexter mechanism [32, 33], on the other hand, is best thought of as two concomitant electron transfer reactions (see Scheme 1.5). Except in rare cases, electron transfer is a through-bond process, meaning that Dexter transfer requires orbital overlap between the donor and the acceptor in order for the energy transfer process to proceed: this limits its occurrence to shorter distances than the Förster mechanism (typically no more than 10 Å). In other words, for a bimolecular reaction the Dexter process requires physical contact between the excited donor and the acceptor. On the plus side, since it is an exchange process (as opposed to a resonance one), no spectral overlap is required.

Molecular oxygen can quench the excited state of many transition-metal polypyridyl compounds via Dexter energy transfer [34, 35]. For this reason, most photophysical measurements involving  $[\text{Ru}(\text{bpy})_3]^{2+}$  and other transition-metal complexes must be carried out in deoxygenated solutions.

## 1.6 Electron Transfer

A generic electron transfer process is represented in Eq. (1.16). In a simple electron transfer reaction (the kind that we are interested in), no bonds are formed or broken; this is known as an outer sphere electron transfer.



The kinetics of outer sphere electron transfer can be described using Marcus theory [36]. In bimolecular systems (such as the ones of interest in organic synthesis), the distance between the donor and the acceptor (as well as their relative orientations) can vary, affecting the rate of electron transfer. For simplicity, we will consider the donor and the acceptor to be at a fixed distance and orientation. Under those conditions, the rate constant for outer sphere electron transfer can be written as shown in Eq. (1.17),

$$k_{\text{eT}} = \frac{2\pi}{\hbar} |H_{\text{AB}}|^2 \frac{1}{\sqrt{4\pi\lambda k_{\text{B}}T}} \exp\left[\frac{(-\Delta G^\circ + \lambda)^2}{4\lambda k_{\text{B}}T}\right] \quad (1.17)$$

where  $\Delta G^\circ$  is the driving force for electron transfer (which depends on the redox potentials of the donor and the acceptor),  $H_{\text{AB}}$  represents the electronic coupling between the donor and the acceptor, and  $\lambda$  is the reorganization energy. This latter term reflects energetics associated with the structural changes in going from reactants to products as well as the reorganization of the solvent molecules around them. The magnitude of the electronic coupling ( $H_{\text{AB}}$ ) depends on the distance and orientation of the donor and the acceptor and therefore tends to be difficult to specify for bimolecular reactions in solution.

Even though electron transfer and Dexter energy transfer are closely related, two important differences should be noted. First, because two electrons are exchanged instead of one, Dexter energy transfer has a stronger distance dependence than electron transfer (typically  $e^{-2r}$  as opposed to  $e^{-r}$  for electron transfer) [33]. Second, since electron transfer leads to a new charge distribution, the reorganization energy (especially the solvent contribution) is much larger than that associated with Dexter energy transfer [37].

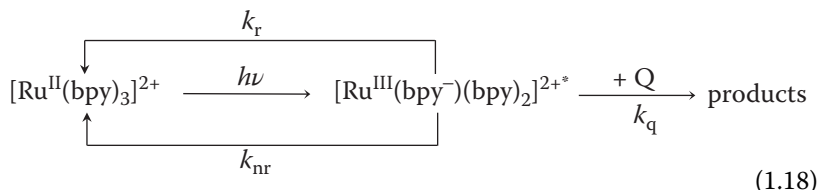
The product of a Dexter energy transfer differs from that of an electron transfer because no charge-separated species is formed. This turns out to be an extremely important distinction that helps differentiate these two reaction pathways, as will be discussed later.

## 1.7 Probing the Mechanism, Stage I: Stern–Volmer Quenching Studies

The simplest experiment that can be performed is a Stern–Volmer quenching study. With this experiment, it is possible to determine whether a bimolecular reaction is taking place. While this is extremely useful information, it is important to stress that this experiment does not provide any mechanistic information by itself. As will become apparent in the discussion to follow, both energy and

electron transfer reactions involving the excited state of the chromophore will yield experimentally indistinguishable results from a Stern–Volmer quenching study. It is only through the application of additional experiments (most notably time-resolved absorption spectroscopy) that further insight into the nature of the reaction responsible for the quenching can be gleaned.

In Section 1.3, the radiative and nonradiative pathways for the excited state were described. When a species other than  $[\text{Ru}(\text{bpy})_3]^{2+}$  is present in solution, the possibility of one or more additional reactions, such as electron and/or energy transfer, is introduced. When this happens, the excited state is quenched (the ground state is recovered). In a very general way, when a quencher is present, we can write the reaction shown in Eq. (1.18).



In this scheme, the rate at which the excited state disappears is given by Eq. (1.19).

$$-\frac{d[\text{ES}]}{dt} = k_0 [\text{ES}] + k_q [\text{ES}][\text{Q}] \quad (1.19)$$

For bimolecular quenching to take place,  $k_q [\text{Q}]$  must be larger than  $k_0$ . This condition is usually met if the excited-state lifetime is on the nanosecond to microsecond time scale. Otherwise, the excited state relaxes back to the ground state before it can diffuse to and react with the substrate (Q) [20]. The goal of Stern–Volmer studies is to determine whether the excited state reacts with the quencher. Quantifying  $k_q$  is most easily done by carrying out the study under pseudo first-order conditions: the concentration of the quencher must be at least two orders of magnitude larger than that of the photocatalyst,<sup>6</sup> so that [Q] can be assumed to be constant throughout the experiment. This collapses Eq. (1.19) to Eq. (1.20) and allows for the determination of  $k_q$  (Eq. (1.21)). The observed rate constant ( $k_{\text{obs}}$ ) varies with the concentration of the quencher.

$$-\frac{d[\text{ES}]}{dt} = (k_0 + k_q[\text{Q}])[\text{ES}] = k_{\text{obs}} [\text{ES}] \quad (1.20)$$

$$k_{\text{obs}} = (k_0 + k_q[\text{Q}]) \quad (1.21)$$

$k_{\text{obs}}$  may be directly determined using time-resolved spectroscopy. If the sensitizer is emissive, this is most easily done via time-resolved emission spectroscopy: by measuring the decay rate constant at several quencher concentrations, the quenching constant  $k_q$  can be found when fitting the results to Eq. (1.22).

$$\frac{k_{\text{obs}}}{k_0} = \frac{k_0 + k_q[\text{Q}]}{k_0} = 1 + \frac{k_q[\text{Q}]}{k_0} \quad (1.22)$$

<sup>6</sup> Strictly, it must be  $[\text{Q}] \gg [\text{ES}]$ , but since evaluating the concentration of the excited state is not trivial, it is simpler to make  $[\text{Q}] \gg [\text{photocatalyst}]$ .

Alternatively, steady-state emission spectroscopy can be employed. In the absence of contributions from static quenching [38], the radiative quantum yield of the photocatalyst in the presence of a quencher depends on  $k_q$ , as shown in Eq. (1.23).

$$\Phi_q = \frac{k_r}{k_0 + k_q[Q]} \quad (1.23)$$

Provided that the radiative quantum yields in the presence and absence of the quencher are measured under identical experimental conditions, their ratio can be related to the Stern–Volmer expression (Eq. (1.24)).

$$\frac{\Phi_0}{\Phi_q} = \frac{I_0}{I_q} = \frac{k_0 + k_q[Q]}{k_0} = 1 + \frac{k_q[Q]}{k_0} \quad (1.24)$$

Assuming that the rate constant for excited-state decay of the chromophore ( $k_0$ ) is known,  $k_q$  can be determined by measuring the radiative quantum yield as a function of quencher concentration.

Stern–Volmer studies are helpful because the excited-state lifetime is shortened if a reaction between the photocatalyst and a quencher takes place. However, the only information these studies can provide is whether or not the excited state is being quenched; ***they do not in any way provide mechanistic insights because energy and electron transfer quenching pathways will yield qualitatively indistinguishable results for this experiment.***

## 1.8 Probing the Mechanism, Stage II: Electron Versus Energy Transfer

The discussion above underscored the extremely important point that a Stern–Volmer study does not provide any insight into the actual reaction the excited state of a sensitizer is engaging in. A simple analogy can be drawn with, for example, a Schiff base condensation. If one used NMR to probe this reaction, the disappearance of the aldehyde proton resonance would never be used as proof that the imine had formed, only that a reaction involving the aldehyde had taken place. In the same way, the observation of quenching of emission from the sensitizer from a Stern–Volmer quenching study is nothing more than evidence that the starting material (i.e., the excited state) is being consumed. In order to determine what reaction actually occurred, one must identify the product(s) of the reaction.

As mentioned previously, the two dominant excited-state reaction pathways available in most systems are electron and energy transfer from the excited state to the substrate; in the case of the former, oxidative and reductive quenching are both possible, with each leading to distinctly different products. In the case of energy transfer, the photocatalyst will go back to the ground state (see Eq. (1.14a)), whereas electron transfer will result in the oxidation or reduction of the photocatalyst (with corresponding reduction or oxidation of the substrate, Eqs. (1.14b and 1.14c)). Direct detection of one (or more) of these products is the gold standard by which mechanistic pathways in these reactions must be established.

Time-resolved absorption spectroscopy, also known as transient absorption (TA), is a very useful tool in these cases. This technique uses a laser pulse to excite the sample and a white light source to probe the absorption of the transient species formed due to excitation, using the absorption of the ground state as the blank. The TA signal is the change in absorbance of the sample before and after excitation. This renders the technique more versatile than time-resolved emission, because non-emissive molecules can be studied as well. Depending on the instrumentation available, difference spectra can be acquired at single wavelengths (yielding kinetic traces, see Figure 1.5) or a full spectrum can be obtained.

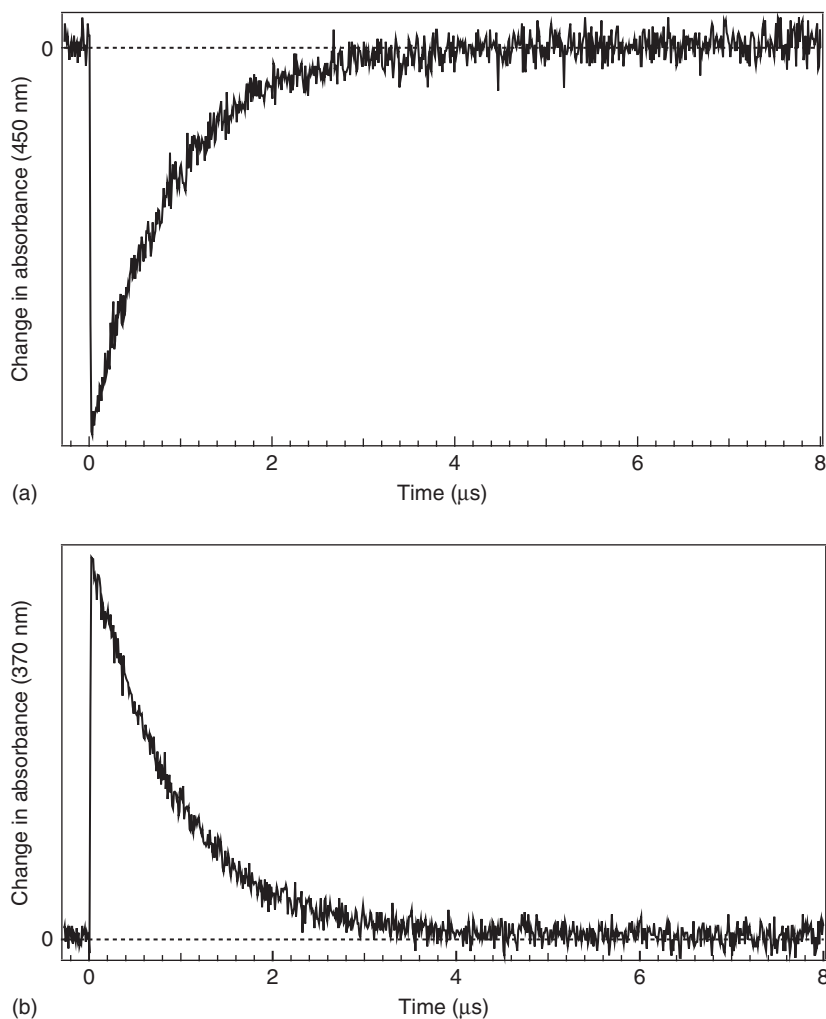


**Figure 1.5** Kinetic traces for  $[\text{Ru}(\text{bpy})_3]^{2+}$  in acetonitrile;  $\lambda_{\text{pump}} = 475 \text{ nm}$ . (a)  $\lambda_{\text{probe}} = 450 \text{ nm}$ ; the bleach is due to the presence of  $\text{Ru}^{\text{III}}$ . (b)  $\lambda_{\text{probe}} = 370 \text{ nm}$ ; this positive feature arises from the reduced ligand. Both traces go back to zero with the same time constant.

For a TA experiment, an expression derived from Beer's law can be written, as shown in Eq. (1.25).

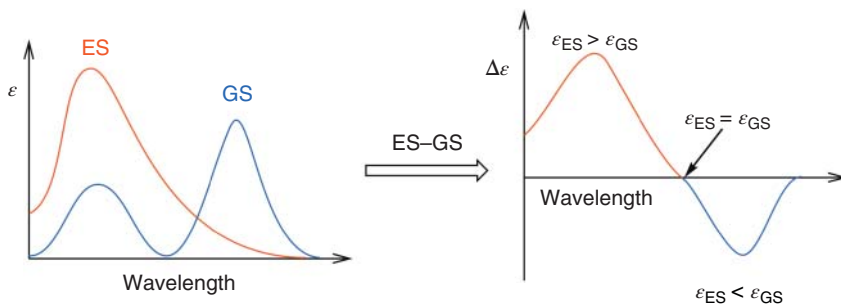
$$\Delta A = \Delta \epsilon \cdot b \cdot [\text{GS}] \cdot \eta^{\text{ex}} \quad (1.25)$$

where  $\Delta A$  is the change in absorbance before and after excitation (i.e., excited state minus ground state),  $\Delta \epsilon$  is the change in molar absorptivity (the difference between the ground state and the excited state),  $b$  is the optical path length,  $[\text{GS}]$  is the concentration of the ground state (the concentration of the sample), and  $\eta^{\text{ex}}$  is the fraction of molecules that are excited from the ground state to the excited state ( $0 < \eta^{\text{ex}} < 1$ ). For a given experiment,  $b$  and  $[\text{GS}]$  are constant.  $\eta^{\text{ex}}$  depends, among other factors, on the cross section between the pump and probe beams, but remains constant as long as the experimental conditions are not changed. When that is the case, any changes in the sign of  $\Delta A$  are a direct reflection of the changes in  $\Delta \epsilon$ .

Scheme 1.7 is a cartoon of a full spectrum obtained in a TA experiment. If at a certain wavelength the excited state absorbs more strongly than the ground state, a positive feature is observed. Conversely, if the ground state absorbs more than the excited state, a negative feature ("bleach") is obtained. The points where the excited and ground states have the same absorbance are called isosbestic points.

For  $[\text{Ru}(\text{bpy})_3]^{2+}$ , it is known that the main feature for the oxidized species is a bleach centered around 450 nm; [39] this signal is diagnostic of the presence of Ru(III). In the case of  $[\text{Ru}(\text{bpy})_3]^+$ , the absorption centered around 370 nm indicates the presence of a bpy radical anion. The kinetic traces at 450 and 370 nm are shown in Figure 1.5: as the excited molecules relax back to the ground state, the features of  $[\text{Ru}(\text{bpy})_3]^{2+}$  are recovered and the kinetic trace goes back to zero.

Now let us consider what happens to the TA traces upon adding a quencher. To illustrate the different scenarios, several simulated TA traces are shown in Figure 1.6. For the unquenched photocatalyst, a lifetime of 700 ns was used. To make comparisons easier, a lifetime of 300 ns was assumed for the quenched photocatalyst, regardless of the reaction taking place. Irrespective of the type of quenching,  $[\text{Ru}^{\text{III}}(\text{bpy}^-)(\text{bpy})_2]^{2+*}$  is formed after excitation, leading to a positive feature at 370 nm (due to  $\text{bpy}^-$ ) and a bleach at 450 nm (diagnostic of  $\text{Ru}^{\text{III}}$ ).



**Scheme 1.7** (b) Schematic representation of a transient absorption plot. The positive feature is shown in red, while the bleach is in blue. (a) Schematic absorption spectra of the ground and excited states.